Mechanics & Industry **21**, 414 (2020)
© AFM, EDP Sciences 2020
https://doi.org/10.1051/meca/2020043

Mechanics & Industry

Available online at:
www.mechanics-industry.org

Regular Article

Aerodynamic control of a diffusion flame to optimize materials' transition in a rotary cement kiln

Mohamed Nial[1,*], Larbi Loukarfi[1], and Hassane Naji[2]

[1] Hassiba Benbouali University, CTMS. Lab, Chlef, B.P. 151, 2000, Algeria
[2] Univ. Artois, Univ. Lille, IMT & Yncréa-HEI, Laboratoire Génie Civil & géo-Environnement (ULR 4515), Technoparc Futura, F-62400 Béthune, France

Received: 28 October 2019 / Accepted: 16 May 2020

Abstract. The aim of this work is to deepen the understanding of the aerodynamics of a diffusion flame in a rotary cement kiln. The kiln is a rotary with a cylindrical shaped, long and equipped with a burner, and it is the seat of a diffusion flame with an axisymmetric turbulent jet. The kiln has a capacity of 8,000 Nm^3 to 13,000 Nm^3 of natural gas and primary air at $T = 25\,°C$ which interacts with a secondary hot air volume at $T = 800\,°C$. The aerodynamic modelling of the furnace is achieved using the turbulence model RNG k–ε, which is able to handle the turbulence and capture the vortex shedding process. The Ansys/Fluent code, based on the finite volume approach to solve the Reynolds averaged Navier-Stokes (RANS), was used in this study. The interactions between turbulence and diffusion flame were handled by the PDF (Probability Density Function) approach. The numerical simulations have been validated by experiments from the kiln considered. Based on the findings obtained, it is concluded that the recirculation zone seems of paramount importance when combustion is taken into account because the reverse flow improves the flame stability and affects the combustion efficiency. In addition, limiting the secondary air flow through the furnace is major to improve combustion and avoid disturbing the advancement of the material along the kiln.

Keywords: kiln shell / sinter ring / turbulent flow / diffusion flame / saltation / CFD

1 Introduction

In recent years, some conventional kilns of dry cement plant have increased their productivity by more than 30%. However, the upgrade of some cement plants can exceed the cost of a new installation. The calciner burners are among the best solutions to improve the kiln production capacity by upgrading the combustion process. The technique consists in introducing a fuel quantity in to the preheater. The raw meal suspended in the preheater cyclone is heated according to the thermal energy used up to the calcination temperature. This technique increases the calcination rate of raw meal before entering the kiln. The increase in flows rates (fuel, primary air, secondary air and raw meal) causes flame instability, the raw meal transition and the clinker advancement. Research in the field has indicated that rotary kilns promote increased gas combustion with diffusion flame instabilities due to the different fluids emanating from the coaxial burner. In addition, the kiln burners are characterized by long diffusion flames, the characteristics of which are strongly affected by the presence or absence of recirculation. The use of diffusion flames in rotary kilns has a rapid effect on the raw meal transformation due to the high rate of heat release, which helps to increase the production of the rotary kiln.

Subhash and Anjan [1] pointed out that the drawback of confined diffusion flames is the heat flow instability generated near the point of stagnation. The confined flame becomes unstable once its shape becomes larger than the freeboard of the kiln. Yagi and Saji [2] stated that it is not always possible to discuss the flames confined in industrial rotary kilns because the secondary air temperature and the interior wall temperature of the kiln strongly depend on the operating conditions of the kiln. The main goal of efficient burners is a stepwise combustion, which delays the mixing and supply of fuel and air at appropriate stages to achieve a controlled combustion process [3]. In reference [4], it has been specified that the appropriate choice of burner design will generate reasonably small combustion zones, avoiding wall impingement and enhance flame stability. For aerodynamic control of the flame, the primary air improves the internal mixing layer of the diffusion flame and installs

* e-mail: m.nial@univ-chlef.dz

a central recirculation zone. In a direct firing system, the external recirculation zones are shifted deeper into the kiln between the resulting jet and the secondary air, gave more efficiency to the diffusion flame [5]. Boateng [5] reported that axial segregation (sequential bands of small and large particles along the length of the furnace) and accretion (growth of material on the refractory wall, forming undesirable barriers) are not well understood and are often described qualitatively. Favalli et al. [6] simulated several configurations of rotary kiln hood and the results confirmed that the penetration of the burner, a few centimetres into the kiln, improves the resulting velocity profile, the temperature profile of the gases and the secondary air volume trained from the cooler to the kiln. For the same primary and secondary air flow rates, and consequently the same swirl, turbulence and impulse indices, tests were carried out to verify how the geometry of the burner nose might improve not only the burner's performance, but also the whole kiln operation [6]. This operation helps to prevent the direct impact of the flame on the clinker bed under unstable conditions to restore the conditions for a good quality clinker. In Ref. [7], authors mentioned that for efficient natural gas combustion, the gas velocity is between 200 m/s and 280 m/s with a slight rotation of the flame. Moreover, they showed that the maximum reaction activity for clinker formation occurs in the middle of the burning zone where the temperature of the flame reaches its peak. High injection velocity causes the fuel to be injected too far into the kiln, and the energy is not released in an appropriate location to contribute to raise the temperature of the clinker [8]. This is an important consideration in the design and operation of many practical systems, notably in rotary kilns. The location of maximum heat release will be closer to the burner for the processing jet flame than for the simple jet flame [9]. The temperature of the wall of the prototype kiln reaches the maximum and remains approximately constant following the experiment, which means that the temperature of the material bed converges with the kiln shell temperature in experimental data published in reference [10]. It is indicated in reference [11] that axial diffusion of the flame has a profound influence on the distribution of localized heat release as well as on the overall asymptotical heat release. The study made in reference [12] about the energy efficiency of kilns in the cement industry concluded that the improvement of combustion is the main parameter for an efficient energy system. In rotary kiln, when cohesion is significant, the formation of agglomerates is inevitably present and affects the combustion in the kiln [13].This explains that the particles are retained in the clinker bed (melting phase) or suspended in the flow gases downstream to form a sinter ring. Yagi and Saji [14] have shown that destructed sinter ring in the upstream transition zone by dilution of the secondary air with fresh airflow induces a shrinkage to the sinter ring under thermal shock. Tsoar and Bagnold [15] had established the saltation principle of particles by wind effect. They had established wind profiles and conducted sand flow measurements on an open dune surface in the Egyptian-Libyan desert. They had found that their measurements match those obtained in the wind tunnel. Fessler et al. [16] invoked that, for a flow loaded with dust at a Stokes number $\gg 1$, the particles are unaltered by the vortex structures. However, for a Stokes number ≈ 1, the particles are altered and do not follow the streamlines. Meanwhile, the particles form agglomerates between the recirculation zones. Hussainov et al. [17] have shown that the rough particles considered in a two-phase flow soften the resulting turbulent flow while amplifying its dissipation energy and attenuating its turbulent kinetic energy. It should be noted that phenomenon of the transport of fine particles are affected by large coherent structures and the flame impulsion.

Fig. 1. Heating kiln with new firebricks.

2 Rotary kiln description

The kiln is the middle part of the burning workshop between preheater and cooler. The most important advantages of the new cement plant compared to a conventional cement plant are that 60% of the total thermal energy is used in the calciner and the remainder in the kiln. The air required in the calciner (tertiary air) is supplied from the cooler bypassing the kiln. On the other hand, the revamped cement plant uses 30% max of the total thermal energy in the preheater. The oxygen rest from the flame combustion in the kiln (Fig. 1) is used in the precalciner combustion. This is a compromise where the flame temperature of the kiln burner decreases when more secondary air (oxygen) is generated in the kiln, as well more dust is transported in the kiln. A stable coating helps protect refractory bricks and preserve kiln production. Figure 1 shows new firebricks without coating, while Figure 2 depicts a kiln with a stable coating. Figure 3 displays a stopped kiln with an exaggerated concretion and a sintering ring downstream the tip burner, altering the transition and the movement of the material. When the cohesion of the material particles is expected due to dusty clinker, a local ring agglomeration is installed, so that the kiln filling is increased. Thereby, the agglomerates are not preserved but have increased in volume. The large clinker particles move towards the cooler, unlike fine particles which follow the streamlines of the gas stream and stick to the inner wall of the kiln. Besides, the kiln rotation favours

Fig. 2. Heated kiln with stable coating.

Fig. 3. Diameter kiln reduction.

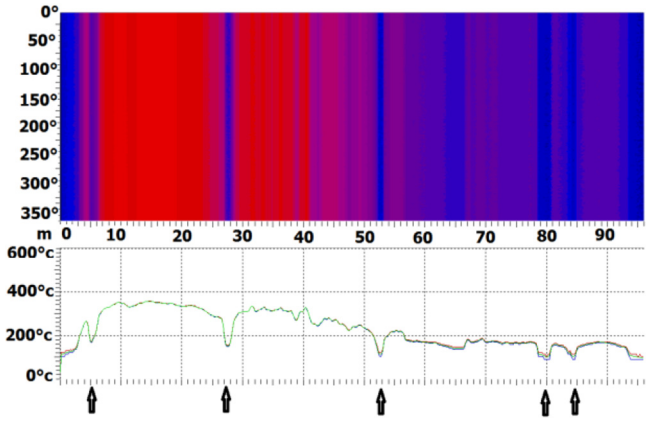

Fig. 4. Shell kiln temperature profile (new firebricks).

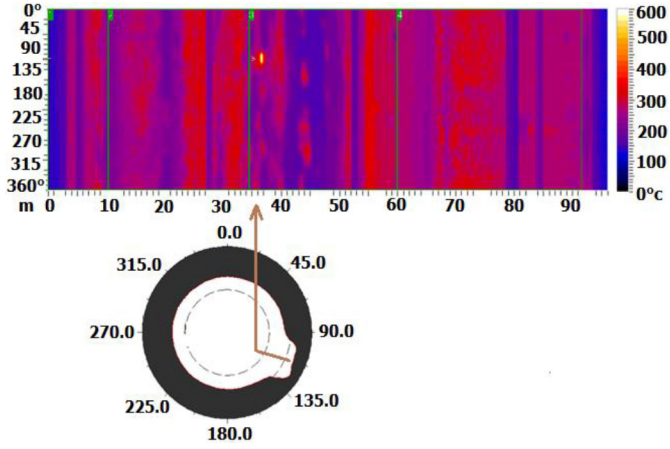

Fig. 5. Estimation of coating thickness of kiln wall with apparition of the red spot.

a homogeneous circular coating along the clinkering process area. The interaction of different flows stream (fuel, primary air and secondary air) downstream the tip burner upon the clinker melting bed is an aerodynamic phenomenon, to which the coating arrangement along the combustion zone (Fig. 2) looks like a dune arrangement in the desert.

During the heating of the new firebricks installed, the kiln shell temperature follows the theoretical temperature profile of the kiln shell (Fig. 4). Hence, since the temperature gradient tends to zero across the clinker bed and the kiln wall, the heat transfer coefficient remains constant. After feeding the kiln, raw meal undergoes a physicochemical transformation along the kiln and a moderate concretion layer is uniformly formed along the zone from 10 m to 60 m downstream from the tip burner depending on the quality of the firebricks.

When the kiln's raw meal bed reaches 25% of the kiln freeboard, a rough coating forms and an unusual sinter ring appears at the beginning of the combustion zone. The reduced freeboard section increases the secondary air velocity, and extends the flame heat release zone. Thereby, it induces aerodynamic excitation to the flame via the flame Strouhal number. The temperature profile of the kiln shell reflects the thickness of the different layers of the kiln wall (shell kiln, firebricks and coating) based on the radiation of the kiln shell.

Thermography measurement of the kiln shell temperature is used to indicate the coating thickness and to predict the apparition of hot spots. In Figure 4, the red, blue and green curves show the maximum, minimum and average of the shell temperature, respectively. The five hollows identified by the arrows (Fig. 4) at positions 7 m, 28 m, 53 m, 84 m illustrate the kiln tires (support), while the hollow at position 80 m shows the girth gear of the kiln drive system. Figure 5 shows multiple sinter rings located in positions 10 m, 20 m and 36 m. Others thicker and larger are located in position 42–49 m, and are identified by the dark blue colour. The red spot (position 36 m) appears after detachment of the concretion block attached to firebrick. Note that the sinter ring disrupts the chemistry of the clinkering process by retaining the clinker melting bed.

The retention of materials behind the sinter ring (dame ring) increases concretion, and once it is overloaded, the concretion block eventually drops and some of the firebricks come off. Finally, when a closet of firebricks comes off, the kiln is stopped.

2.1 The practical case

Figure 6 shows the time evolution and alteration of the concretions in the burning zone. Four sinter rings were identified, the first is located at 23 m, the second at 30 m, the third at 43 m and the forth at 60 m.

A few hours after checking the primary air impulsion, there is a progressive fall of portions of the sinter ring located from 35 m−45 m, while a new sinter ring is formed at 30 m and after that at position 40 m. In the 58 m−65 m zones, the coating is unstable and the sintering ring is less linked to refractory bricks. This is why, during the alteration, the temperature profile of the kiln shell evolves smoothly in this zone. The excitation of the flame jet generates a new recirculation zones distribution in the combustion zone. Thereby, the flame front displacement induces periodic thermal shocks thus yielding a blocks shrinking of sintering rings. As a result, a hot spot appears (see the last image in Fig. 6). The fall of the sintering ring provides additional materials in the kiln, which added to the combustion zone increases the combustion time, lowers the flame temperature and gives rise to a dusty clinker. The distribution of the flame heat release, the clinker residence time delay and the exothermic heat release in the burning zone intensify the firebricks deterioration risk (250 °C of kiln shell temperature being the advised temperature for safe operating of the kiln). An external air cooling system is used to handle the kiln shell temperature as can be seen through recording videos of several days and months of kiln monitoring.

3 Computational methodology

When modelling combustion, the flame is often idealized as an axi-symmetrical turbulent jet diffusion flame, consisting of a fuel jet issuing into a concentric confining cylinder with a surrounding air co-flow. So, for statistically axisymmetric and stationary flows such as coaxial jets, the governing equations are considered in cylindrical coordinates. Explicitly, it is the RANS (Reynolds Averaged Navier Stokes) approach which is adopted herein where only mean flow fields are resolved. Note that, the pressure field is get via the velocity-pressure coupling, called the SIMPLE algorithm. Although radiation is considered to be moderate in the combustion of natural gas compared to convection and conduction, the P1 model for the radiation transfer mode was used here. The interactions between turbulence and diffusion flame are handled via the PDF (Probability Density Function). Note that, in the Ansys Fluent software, non-adiabatic extensions of the PDF model are required [18] to study the systems comprising several fuel or oxidant inlets with different inlet temperatures. The mesh refinement near walls does not seem necessary since the experiment within simple geometries (case of the rotary kiln) can be easily carried out. It should be specified that zones affected by the viscosity is not resolved, but filled in using wall function approaches, which are often adopted in flows at large Reynolds numbers. For a valid logarithmic velocity profile, the first grid point far from the wall can be located at parietal coordinate $y^+ > 30-40$.

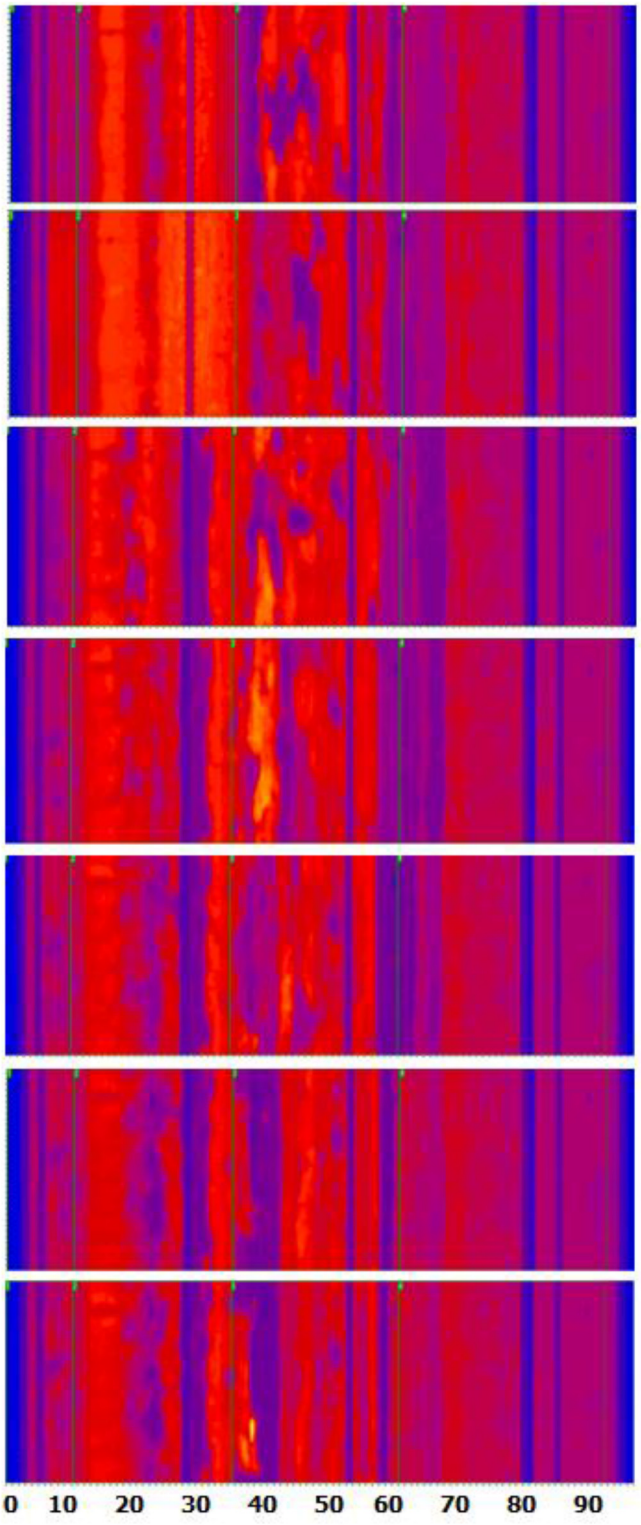

Fig. 6. Time series images of a kiln shell temperature (ECDE).

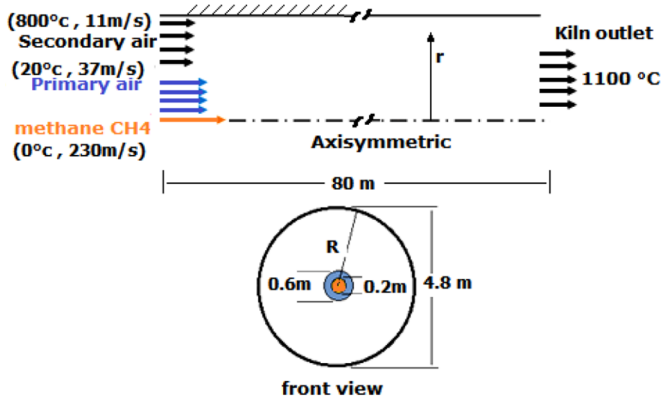

Fig. 7. Geometry dimensions with initial conditions.

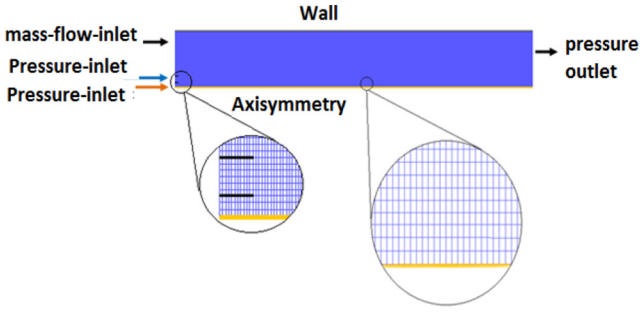

Fig 8. Quadrilateral mesh elements with boundary conditions.

Figure 7 depicts the initial and boundary conditions of the geometry considered in our study, while Figure 8 illustrates the geometry meshed in regular quadrilateral elements along with boundary conditions (BCs). Note that CH_4 arrives through the central inlet, while air arrives through the primary and secondary entrances. As for the outlet, it is on the right where boundary conditions of the preheater are prescribed.

The principal of coherent structure formation has been often studied [19] based on relative velocities between fuel and air streams. When the fuel jet has sufficient momentum to prevent the flow reversal along its axis, the fuel stream may be influenced by the surrounding buoyancy, in particular by surrounding hot gases (secondary air) thereby, causing an ambient fluid into the flame. Since the flow rates considered are those of a real case, we used initial conditions (burner parameters and fluid inputs) for the ECDE (*Entreprise des Ciment et Dérivées d'Echlef, algeria*) kiln. In other words, the fluids velocity is predefined (Fig. 7) as being high in the center of the coaxial jet (230 m/s) and lower in the peripheral jets (37 m/s and 11m/s, respectively). As for temperatures, that of natural gas is below 1 °C, that of primary air varies between 10 °C in winter and 40 °C in summer, and that of secondary air (hot recovery air) varies between 600 °C and 900 °C depending on the temperature and the amount of clinker in the cooler. In accordance with our reactions system, the non-adiabatic non-premixed model [18] was adopted.

3.1 Assumptions

As up-stated, the flow is considered as steady. The gas used is pure methane and combustion is based on the fast chemical equilibrium chemistry assumption [20]. The gases around the flame are transparent to radiation. The walls are assumed to be stationary and the raw meal in the kiln is negligible compared to the kiln free board. Since the heat losses have no significant impact on the turbulent enthalpy fluctuations, the system is assumed to be adiabatic. Furthermore, the thermal capacities of matter particles are assumed to be negligible compared to those of combustion gases ($C_{p(particles)} \ll C_{p(gases)}$). As a result, the heat absorbed by the particles is instantly transferred to the gas, thereby avoiding solving the particle temperature equation according to Ref. [21].

It is worth noting that, in the stochastic tracking approach, the ANSYS Fluent software predicts the particles turbulent dispersion using the trajectory equations for individual particles with the instantaneous fluid velocity.

3.2 Turbulence model

The Renormalization Group (RNG) k-epsilon turbulence model, derived from the theory of renormalization group, has proven to be able to better model confined jets compared to the standard $k-\varepsilon$ model. The model describes the rapid dynamic changes within the flow, in particular the streamlines' inflection. Computing using this model takes 10 to 15% more CPU time than the standard $k-\varepsilon$ model, but it provides more realistic results for engineering applications.

For 2D axisymmetric geometry, the turbulent kinetic energy "k" and its dissipation rate "ε" can be expressed as:

$$\frac{1}{r}\frac{\mathrm{d}(ru_r k)}{\mathrm{d}r}+\frac{\mathrm{d}(u_x k)}{\mathrm{d}x} = \frac{1}{r}\frac{\mathrm{d}}{\mathrm{d}r}\left[\alpha_k \mu_t r\frac{\mathrm{d}k}{\mathrm{d}r}\right]+\frac{\mathrm{d}}{\mathrm{d}x}\left(\alpha_k\,\mu_t\frac{\mathrm{d}k}{\mathrm{d}x}\right)+\alpha_k\,\mu_t\frac{k}{r^2}+\mu_t S^2-\varepsilon \quad (1)$$

$$\frac{1}{r}\frac{\mathrm{d}(r\varepsilon u_x)}{\mathrm{d}r}+\frac{\mathrm{d}(\varepsilon u_r)}{\mathrm{d}x} = \frac{1}{r}\frac{\mathrm{d}}{\mathrm{d}r}\left[\alpha_\varepsilon\,\mu_t r\frac{\mathrm{d}\varepsilon}{\mathrm{d}r}\right]+\frac{\mathrm{d}}{\mathrm{d}x}\left[\alpha_\varepsilon\,\mu_t\frac{\mathrm{d}\varepsilon}{\mathrm{d}x}\right] +\alpha_\varepsilon\,\mu_t\frac{k}{r^2}+C_{1\varepsilon}\frac{\varepsilon}{\rho k}-C_{2\varepsilon}\frac{\varepsilon^2}{\rho k}-\frac{1}{\rho}R_\varepsilon \quad (2)$$

where,

$$R_\varepsilon=\frac{C_\mu\rho\,S^3k^2\varepsilon(\eta_0\,\varepsilon-Sk)}{\eta_0\left(\varepsilon^3+\beta\,S^2k^3\right)} \quad (3)$$

$$\eta=S\frac{k}{\varepsilon} \quad (4)$$

$$S^2=2\left(\frac{\mathrm{d}u_r}{\mathrm{d}r}\right)^2+2\left(\frac{\mathrm{d}u_x}{\mathrm{d}x}\right)^2+\left(\frac{\mathrm{d}u_r}{\mathrm{d}x}+\frac{\mathrm{d}u_x}{\mathrm{d}r}\right)^2 \quad (5)$$

Table 1. Mass fractions of species at kiln outlet [23].

Species	Open FOAM (PaSR)	ANSYS fluent (EDC)	Our simulation (PDF)
CO_2	0.1467	0.1455	0.1425
H_2O	0.1201	0.1191	0.1175
CH_4	0.0339	0.0353	0.0473
O_2	0.0001	0.0016	0.0001

The constants model $C_{1\varepsilon}$, $C_{2\varepsilon}$, α_k, α_ε, μ_0, β, α_0, have the values of 1.42, 1.68, 1.0, 1.39, 4.38, 0.012, 1, respectively. α_k and α_ε are the turbulent inverse Prandtl numbers of k and ε, respectively. Note that, additional terms change dynamically with the turbulence intensity while improving the accuracy of predicting flow deformation and anisotropy of large vortex structures [22]. The turbulent viscosity is computed using the following relationship:

$$\mu_t = \rho C_\mu \frac{k^2}{\varepsilon} \tag{6}$$

The inverse Prandtl numbers α_k and α_ε are among the most important parameters of the RNG k–ε model, which represent the flow energy cascade. For large Reynolds numbers, these quantities are approximately 1.393.

Another advantage of the RNG k–ε model is that α varies as a function of the effective viscosity, which is confirmed by experience. They can be deduced from the following formulas:

$$\frac{\mu_{mol}}{\mu_{eff}} = \left|\frac{\alpha - 1.3929}{\alpha_0 - 1.3929}\right|^{0.6321} \left|\frac{\alpha + 2.3929}{\alpha_0 + 2.3929}\right|^{0.3679} \tag{7}$$

where $\alpha_0 (= \mathrm{Pr}^{-1})$.

4 Results and discussions

This section reviews and comments the main findings of the study. Before that, the sensitivity of the grid resolution was undertaken via simulations using finer grids with 40,000, 63,000, 70,000 and 83,000 cells. It turned out that the differences were negligible as can be seen in Figure 9. It should be recalled that the checking of the achievement of a final solution is based on the convergence of the equations conservation (mass, momentum and energy). Thus, convergence is considered as being achieved when these residuals become less than 10^{-5}. The difference in area-weighted of CH_4 mass fraction, of the CO_2 mass fraction, of the H_2O mass fraction and of the O_2 mass fraction remains less than 2%. The species mass fractions at the kiln inlet are in agreement with the results of the simulation performed (see Table 1, [23]) while corroborating the above grid resolution choice.

From the Figure 10, it is clear that the model successfully predicts the gas temperature profiles at the kiln centreline. The peaks flame temperature are located in two distinct zones, which are identified by a high heat

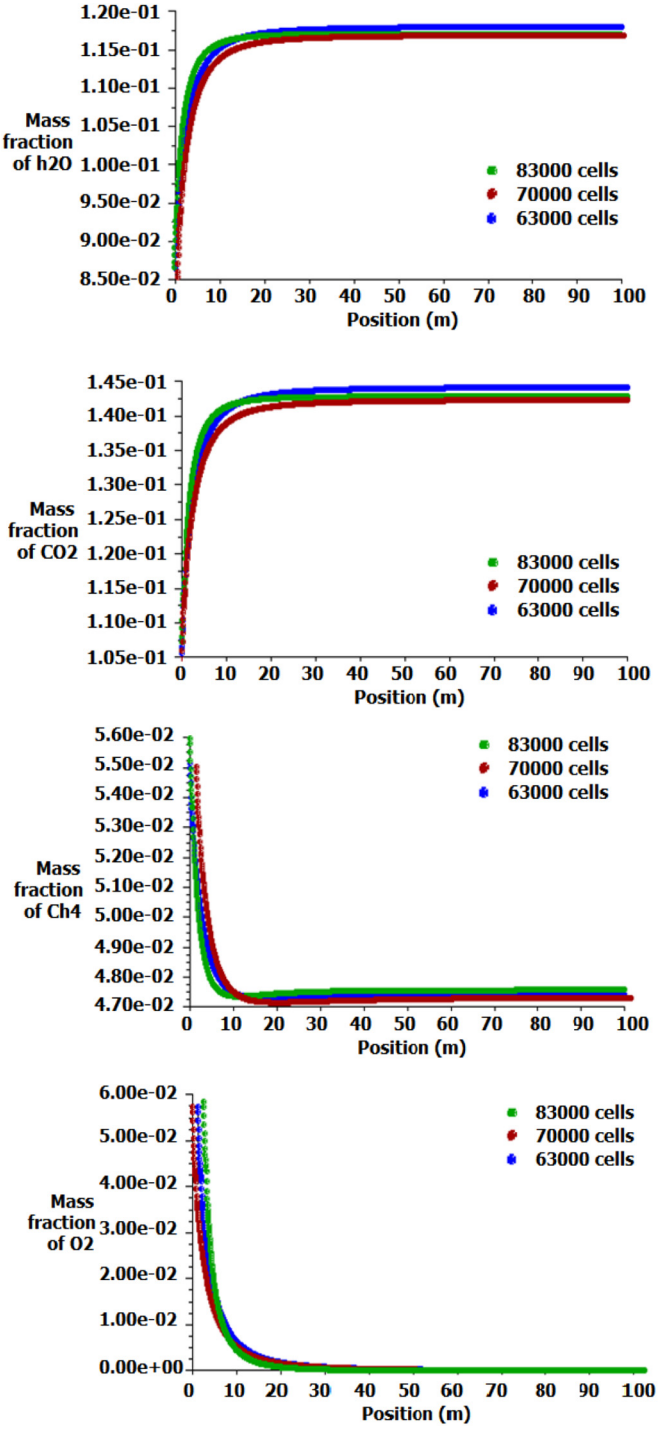

Fig. 9. Grid independence test interpreted by the mass fraction of global one-step reaction mechanism.

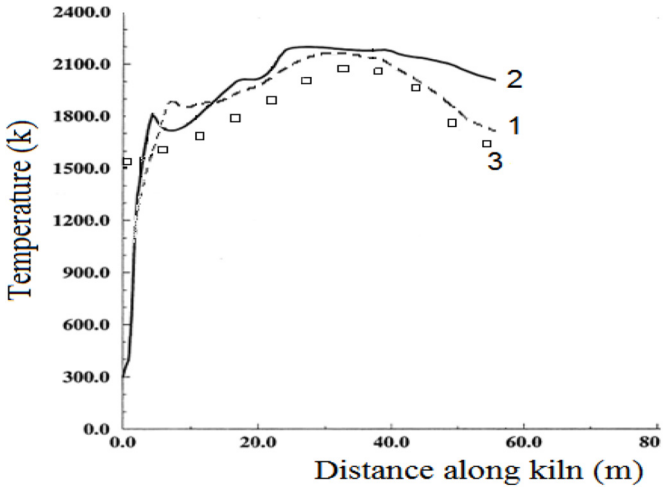

Fig. 10. Comparison of gas temperature profile. 1–Simulated gas temperature profile; 2–Mastorakos et al. [24]; 3–Mujumdar and Ranade [25].

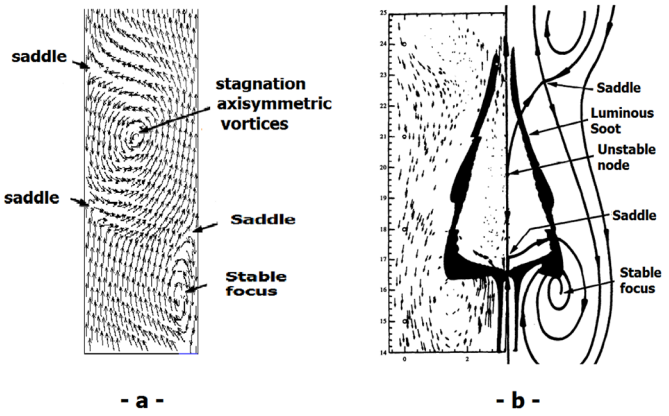

Fig. 11. (a) Flow pathlines, (b) Sketch of flame topology superimposed on the reversed luminous image (right) shown alongside the corresponding velocity vector field (left) for a 45 ° phase angle [26].

release from the flame occurring from 1m to 10 m (zone 1) and from 20 m to 50 m (zone 2). The first temperature peak is due to lower stoichiometric conditions of the mixture (methane and primary air) near the tip burner (zone 1). Therefore, the development of hydrodynamic instabilities in the central fuel jet is delayed considerably by the presence of the surrounding hot gases with their high kinematic viscosity [19]. As for the second temperature peak, it is due to a second time combustion of the flame due to the secondary stream downstream the tip burner (zone 2). Consequently, heat release is important due to large mixing zone of hot secondary air and the product of the first combustion. The predicted temperature profile exhibited on curve 1 in Figure 10 is approximately the same of that of curves 2 and 3. The low enthalpy of the primary air explains the temperature of 1900 K in zone 1. The second combustion is deeply shifted into the zone 2 where the temperature attained 2200 K because of the reactants' high enthalpy. The temperature profile was compared and validated under experimental conditions similar to reference [24] where the Reynolds numbers and kiln dimensions are comparable. Several studies have demonstrated that the maximum temperatures range of the flame in the rotary kiln free board is from 1900 K to 2400 K according to the type of fuel used.

It was found that, the high temperature in zone 2 (Fig. 10) coincides with that of the zone of the clinkering process, as indicated in reference [25].

In addition, the location of the high temperature zone along the kiln is independent from the burner power, but it depends on the velocity generated by the diffusion flame and the kinetic energy dissipation. Recall that the role of a burner is manifold: improve the secondary air intake in the kiln, allow a high turbulence intensity, induce a recirculation zone and produce low NOx emissions. With a very large air-stream momentum much greater than that of the fuel stream, the entire burner operates aerodynamically as a bluff body with a reverse flow along the central axis [19]. This phenomenon is illustrated in Figure 11a–b near the flame zone (attached jet flame in the tip burner) where fuel and hot combustion products are drawn upstream from the low velocity region surrounding the tip burner to establish a second combustion activity centre in the secondary air recirculation. Note that Figure 11a compares favorably with Figure 11b. They exhibit and compare the structures of the flames as a function of the reaction zone attached to the tip burner where the jet flame remains laminar at a considerable height [19]. The hot gases form an annular jet with a second set of axisymmetric vortices at the interface between the hot gases and the fuel flow. These inner vortices rotate in the opposite direction to those outside the reaction zone and are generally much smaller. Note that the flow pattern near the flame base has a saddle point on the centerline that feeds entrained fluid into a large toroidal vortex surrounding the flame stem, as shown in both Figures 11a-b [26]. It is known that particles of a given size behave as fluid flow indicators [27].

The saddle region near the side wall (Fig. 12a) is a particles agglomeration zone that makes think about the location of formation of the sintering ring in the burning zone of Figure 6. In the reality, according to the phenomenon of saltation at low stokes number, the clinker fine particles stick in the combustion zone where materials forming the sintering ring melt. Those are identified by the saddle region between vortices located in hot zones where high rate of the stream function (red colours) shows a high momentum recirculation alley. For the planar injection of parallel jets, the shear flow gives rise to a swirling alley, as reported in [28]. After that, a core of burnt gases is then formed which increases over time [28]. By analysing the pathlines coloured by strain rate (Fig. 12b), the high strain is located in the centreline, downstream of the tip burner in the second axisymmetric vortex ring (the largest). This explains an injection of the fuel further downstream, thereby allowing a completely homogeneous mixture where the secondary flame reaction occurs (zone 2).

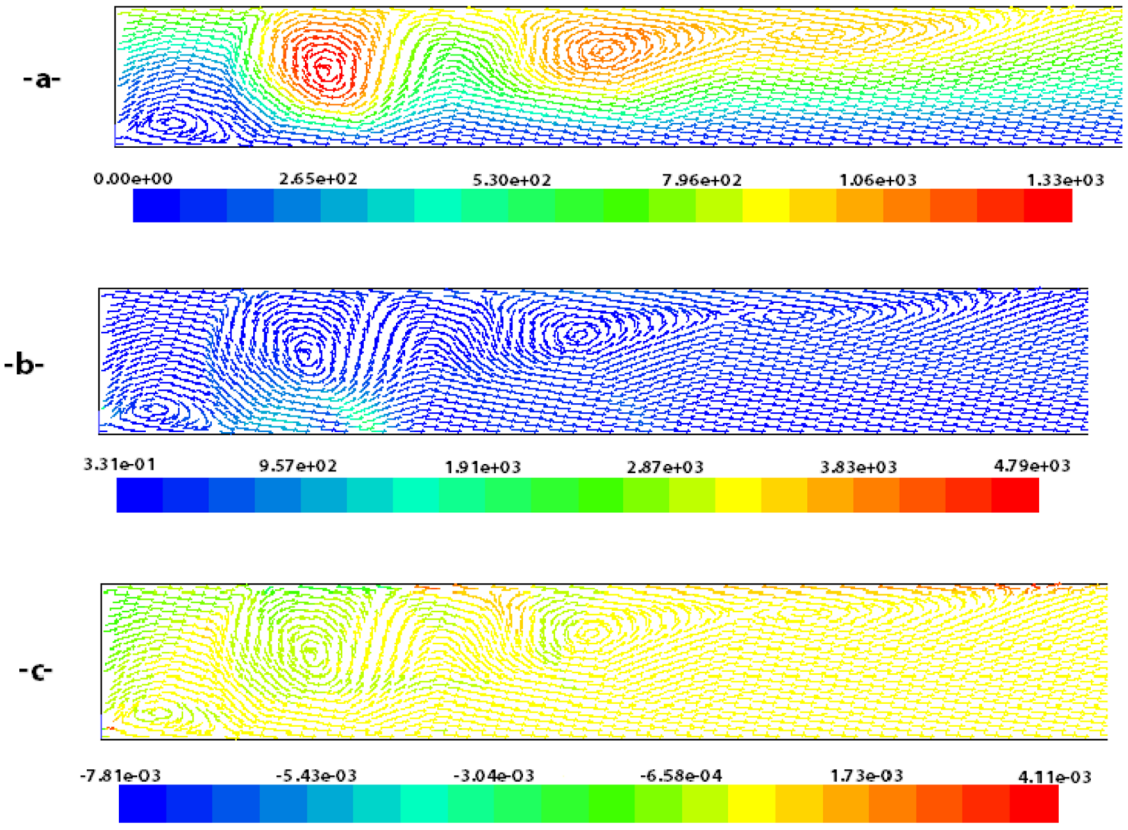

Fig. 12. (a) Pathlines colored by stream function (kg/s); (b) Pathlines colored by strain rate (1/s); (c) Pathlines colored by mass imbalance (kg/s).

It has been reported that an infinitely fast chemistry (equilibrium) leads to structures independent on the strain rate applied to the flame [29]. However, in Figure 12b, the high strain rate coincides with the collapse of the temperature profile between zones 1 and 2. Inside the temperature peak zones (Fig. 10), it coincides with the flame instability zone (separation/attachment behaviour). In other words, the increase in mixing rate in the interface undergoing positive strain is accompanied by a dissipation rate increase, which locally lower the temperature and, thereby the reaction rate [19]. Following this, the extinction occurs when each induced vortex is strong enough to cause a localized reversal of the flow in the fuel flow where the fuel leak reduces the Damkohler number (the almost constant extinction condition corresponding to the Damkohler's number minimum) [30]. Also, it has been mentioned that relatively high local deformation rates, produced by the vortical movement, can be found in a region where the flame extinction takes place (see Ref. [26] for more details). Note that the results shown in Figure 12b reinforced by the mass imbalance results depicted in Figure 12c are sufficient to assess the combustion zone effective length. In addition, Prud'home [28] had mentioned that the Kolmogorov vortices are effective in inducing strain. Since they have a short lifetime due to viscous dissipation, they are unlikely to be able to effectively extinguish the flame.

5 Conclusion

The model presented involves several industrial benefits. Especially, for revamped conventional kilns with a dry process. It allows the development of the resultant turbulent flow in rotary kiln where the transfer of energy from large scales to small scales is highly considered. The location and highlighting of the energy cascade in the kiln allows to better specify the flow initial conditions in the kiln entry, as well as the prediction of the temperature profile of the kiln shell.

Analysis of numerical results from the turbulent flow field demonstrated that temperature peaks are closely related to heat release of the second stream combustion and to the radial flow intensity along the kiln. The aerodynamic control of the non-premixed flame influences directly the kinetic energy and its dissipation rate along the kiln and indirectly influences the sinter rings formation. Hence, limiting the secondary airflow through the kiln is important to improve combustion and to avoid the disruption of the material advancement along the kiln by ensuring a high strain rate in the reaction zone in a burner-attached jet diffusion flame, specially under loaded flow with dusty clinker.

To sum up, in terms of turbulence modelling, the Reynolds baseline stress model (abbreviated as BSL) [18,31] could be used since it is a good trade-off between the computational effort and the targeted flow details.

Nomenclature

C_μ	RNG-$k-\varepsilon$ model coefficient
C_p	Specific heat capacity [J·kg^{-1}·K^{-1}]
K	Kinetic energy [J·kg^{-1}]
Pr	Prandtl number
r	Radial coordinate [m]
S	Mean strain rate tensor [s^{-1}]
u_r	Mean radial velocity [m·s^{-1}]
u_x	Mean axial velocity [m·s^{-1}]
y^+	Wall distance, dimensionless
α_0	Inverse Prandtl number
ε	Dissipation energy [m^2·s^{-3}]
λ	Thermal conductivity [W·m^{-1}·K^{-1}]
μ	Dynamic viscosity [kg·m^{-1}·s^{-1}]
μ_t	Turbulent viscosity [kg·m^{-1}·s^{-1}]
μ_{mol}	Molecular viscosity [kg·m^{-1}·s^{-1}]
μ_{eff}	Effective viscosity [kg·m^{-1}·s^{-1}]
η	Ratio of turbulent to mean strain time scale [J·s^2·kg^{-1}·m^{-2}]
ρ	Mass density [kg·m^{-3}]

Acknowledgment. The first author deeply thanks Professors L. Loukarfi and H. Naji for their unwavering help and support, as well as those who helped him to achieve this work. Special thanks to the ECDE technicians for their continual help.

References

[1] C. Subhash, R. Anjan, An experimental and numerical study of stagnation point heat transfer, for methane/air laminar flame impinging on a flat surface, Int. J. Heat Mass Transfer **51**, 3595–3607 (2008)
[2] S. Yagi, D.K. Saji, Problems of turbulent diffusion and flame jet, Int. Symp. Combust. **4**, 771–781 (1953)
[3] M.H. Vaccaro, Low NO_x rotary kiln burner technology, design principles and case study, in Proceeding of IEEE-IAS/PCA 44th Cement Industry Technical Conference, Jacksonville, Florida, 2002, 265–270
[4] A. Sobiesiak, S. Rahbar, H.A. Becker, Performance characteristics of the novel low-NO_x CGRI burner for use with high air preheat, Combust. Flame. **115**, 93–125 (1998)
[5] A.A. Boateng, Rotary Kilns, Transport Phenomena and Transport Processes, 2nd edition, Elsevier (2015)
[6] R.C. Favalli, L.F. Fabiani, L.F. De Pinho, Enhancing the performance of kiln burner, in world cement, Brazil (2015) 111–117. http://www.dynamis-br.com/files/05-Article_World_Cement_November_2015_D-Flame.pdf
[7] V.K. Klassen, A.G. Novosyolov, I.N. Borisov, V.M. Konovalov, Management of clinker burning in the rotary kiln, aimed to improve the quality of cement and fuel economy, Middle-East J. Sci. Res. **15**, 1871–1876 (2013)
[8] M.N. Pedersen, M. Nielsen, S. Clausen, P.A. Jensen, L.S. Jensen, K. Dam-Johansen, Imaging of flames in cement kilns to study the influence of different fuel types, Energy Fuels **31**, 11424–11438 (2017)
[9] G.J. Nathan, J. Mi, Z.T. Alwahabi, G.J.R. Newbold, D.S. Nobes, Impacts of a jet's exit flow pattern on mixing and combustion performance, Progr. Energy Combust. Sci. **32**, 496–538 (2006)
[10] F. Herz, M. liyan, S. Eckehard, S. Rayko, Influence of operational parameters and material properties on the contact heat transfer in rotary kilns, Int. J. Heat Mass Transfer. **55**, 7941–7948 (2012)
[11] N.A. Magina, T.C. Lieuwen, Effect of axial diffusion on the response of diffusion flames to axial flow perturbations. Combust. Flame **167**, 395–408 (2016)
[12] A. Atmaca, R. Yumrutas, Analysis of the parameters affecting energy consumption of a rotary kiln in cement industry, Appl. Therm. Eng. **66**, 435–444 (2014)
[13] C.G. Ilea, P. Kosinski, A.C. Hoffmann, Simulation of a dust lifting process with rough walls, Chem. Eng. Sci. **63**, 3864–3876 (2008)
[14] M. Pisaroni, R. Sadi, D. Lahaye, Counteracting ring formation in rotary kilns, Math. Ind. **2**, 1–19 (2012)
[15] H. Tsoar, Bagnold RA 1941: The physics of blown sand and desert dunes. London: Methuen, Haim Tsoar, Progr. Phys. Geogr. **18**, 91–96 (1994)
[16] J.R. Fessler, D.K. Jonathan, J.K. Eaton, Preferential concentration of heavy particles in a turbulent channel flow, American Institute of Physics, Phys. Fluids. **6**, 3742–3749 (1994)
[17] M. Hussainov, A. Kartushinsky, A.U. Rudi, I. Shcheglov, G. Kohnen, M. Sommerfeld, Experimental investigation of turbulence modulation by solid particles in a grid-generated vertical flow, Int. J. Heat Fluid Flow. **21**, 365–373 (2000)
[18] Ansys, inc, ANSYS Fluent Theory Guide, release 15.0, USA, 2013. https://www.academia.edu/33546431/ANSYS_Fluent_Theory_Guide
[19] C.M. Coats, Coherent structures in combustion, Energy Combust. Sci. **22**, 427–509 (1996)
[20] N. Peters, Turbulent combustion, Cambridge Monographs on Mechanics, Cambridge University Press, Cambridge (2000)
[21] W. Mingyue, L. Bin, L. Yiqin, W. Shibo, Q. Shan, Z. Aimin, Numerical simulation of oxy-coal combustion in a rotary cement kiln, Appl. Therm. Eng. **103**, 491–500 (2016)
[22] Z. Han, R.D. Reitz, Turbulence modelling of internal combustion engines using RNG $\kappa-\varepsilon$ models, Combust. Sci. Technol. **106**, 267–295 (1995)
[23] A.H. Kadar, Modelling turbulent non-premixed combustion in industrial furnaces, PhD Thesis, Delft University of Technology, Melweg, Netherlands, 2015
[24] E. Mastorakos, A. Massias, C.D. Tsakiroglou, D.A. Goussis, V.N. Burganos, A.C. Payatakes, CFD predictions for cement kilns including flame modelling, heat transfer and clinker chemistry, Appl. Math. Model. **23**, 55–76 (1999)
[25] K.S. Mujumdar, V.V. Ranade, Simulation of rotary cement kilns using a one-dimensional model, Chem. Eng. Res. Des. **84**, 165–177 (2006)
[26] G.S. Lewis, B.J. Cantwell, U. Vandsburger, C.T. Bowman, An investigation of structure of a laminar Non-premixed flame in an unsteady vortical flow, Int. Symp. Combust, 515–522, (1988)

[27] A. Issakhov, R. Bulgakov, Y. Zhandaulet, Numerical simulation of the dynamics of particle motion with different sizes, Eng. Appl. Comput. Fluid Mech. **13**, 1–25 (2019)
[28] R. Prud'homme, Flows of reactive fluids − FMIA Series Vol. 94, Springer, New York Dordrecht, Heidelberg London, 2010
[29] Th. Poinsot, D. Veynante, Theoretical and numerical combustion, 2001 R.T. Edwards Ed., Philadelphia, 2001
[30] F.A. Williams, The Fundamental Theory of Chemically Reacting Flow Systems, Second Edition, Benjamin/ Cummings Publishing Company, Inc., Menlo Park, 1985
[31] R.M.A. Masood, C. Rauh, A. Delgado, CFD simulation of bubble column flows: An explicit algebraic Reynolds stress model approach, Int. J. Multiphase Flow **66**, 11–25 (2014)

Cite this article as: M. Nial, L. Loukarfi, H. Naji, Aerodynamic control of a diffusion flame to optimize materials' transition in a rotary cement kiln, Mechanics & Industry **21**, 414 (2020)